Applied Catalysis B: Environmental 108–109 (2011) 117–126

Contents lists available at SciVerse ScienceDirect

Applied Catalysis B: Environmental

journal homepage: www.elsevier.com/locate/apcatb

$Ce_{0.67}Fe_{0.33}O_{2-\delta}$ and $Ce_{0.65}Fe_{0.33}Pt_{0.02}O_{2-\delta}$: New water gas shift (WGS) catalysts

N. Mahadevaiah, Preetam Singh, Bhaskar Devu Mukri, Sanjit K. Parida, M.S. Hegde*

Solid State and Structural Chemistry Unit, Indian Institute of Science, Bangalore, 560012, India

ARTICLE INFO

Article history:
Received 31 May 2011
Received in revised form 22 July 2011
Accepted 13 August 2011
Available online 22 August 2011

Keywords:
WGS reaction
Oxygen storage capacity
$Ce_{1-x}Fe_xO_{2-\delta}$
$Ce_{1-x}Fe_xPt_yO_{2-\delta}$
WGS catalysts

ABSTRACT

$Ce_{0.65}Fe_{0.33}Pt_{0.02}O_{2-\delta}$ and $Ce_{0.67}Fe_{0.33}O_{2-\delta}$ have been synthesized by a new low temperature sonochemical method using diethylenetriamine as a complexing agent. Due to the substitution of Fe and Pt ions in CeO_2, lattice oxygen is activated in $Ce_{0.67}Fe_{0.33}O_{2-\delta}$ and $Ce_{0.65}Fe_{0.33}Pt_{0.02}O_{2-\delta}$. Hydrogen uptake studies show strong reduction peaks at 125 °C in $Ce_{0.65}Fe_{0.33}Pt_{0.02}O_{2-\delta}$ against a hydrogen uptake peak at 420 °C in $Ce_{0.67}Fe_{0.33}O_{2-\delta}$. Fe substituted ceria, $Ce_{0.67}Fe_{0.33}O_{2-\delta}$ itself acts as a catalyst for CO oxidation and water gas shift (WGS) reactions at moderate temperatures. The rate of CO conversion in WGS with Pt free $Ce_{0.67}Fe_{0.33}O_{2-\delta}$ is 2.8 $\mu mol\, g^{-1}\, s^{-1}$ at 450 °C and with Pt substituted $Ce_{0.65}Fe_{0.33}Pt_{0.02}O_{2-\delta}$ is 4.05 $\mu mol\, g^{-1}\, s^{-1}$ at 275 °C. Due to the synergistic interaction of the Pt ion with Ce and Fe ions in $Ce_{0.65}Fe_{0.33}Pt_{0.02}O_{2-\delta}$, the catalyst showed much higher activity for CO oxidation and WGS reactions compared to $Ce_{0.67}Fe_{0.33}O_{2-\delta}$. A reverse WGS reaction does not occur over $Ce_{0.65}Fe_{0.33}Pt_{0.02}O_{2-\delta}$. The catalyst also does not deactivate even when operated for a long time. Nearly 100% conversion of CO to CO_2 with 100% H_2 selectivity is observed in WGS reactions even up to 550 °C.

1. Introduction

The production of pure hydrogen by a heterogeneously catalyzed water gas shift (WGS) reaction ($CO + H_2O \rightarrow CO_2 + H_2$) is a key step towards realising clean energy by hydrogen–oxygen fuel cells. There are a number of studies on precious metals supported ceria showing much higher catalytic activity than Cu/ZnO [1–5]. On Pt, Pd, Rh metal impregnated CeO_2, CO adsorbed on metals was shown to extract lattice oxygen from CeO_2 and subsequently replace oxygen by H_2O releasing hydrogen [1]. Au and Pt ions in association with CeO_2 were shown to be more active than the corresponding metal on CeO_2 [6–8]. Hydrogen production via formate and carboxilate has also been proposed [3,9]. Deactivation due to surface carbonate formation is a serious issue in WGS catalysis and this has been addressed to a small extent [10,11]. Deactivation of WGS catalyst is more important and a lot of studies have been reported by Flytzani-Stephanopoulos's group [12–18].

We have been pursuing studies on noble metal ionic catalysts (NMIC) where adsorption sites are noble metal ions substituted in CeO_2 and TiO_2 instead of noble metals impregnated in oxide surfaces [19]. Specifically, Pt ion substituted TiO_2 and CeO_2 have shown high rates of CO conversion to H_2 by WGS [20,21]. By making the catalyst surface more acidic, the adsorption of acidic CO_2 forming CO_3^{2-} can be reduced and indeed, Pt^{2+} ion substituted TiO_2 is found to be a highly active non-deactivating catalyst [20]. By the substitution of Ti^{4+} and Sn^{4+} ions in CeO_2, the acidity of the oxide surface can be increased. Fajan's ratio is a measure of acidity of ions given by the charge to radius ratio [22]. Sn^{4+} and Ti^{4+} ions are highly acidic with Fajan's ratios 58 and 61 ($4/r_{Sn^{4+}} = 58; 4/r_{Ti^{4+}} = 61$) respectively compared to 40 for the Ce^{4+} ion ($4/r_{Ce^{4+}} = 40$) [22]. Also Ti and Sn ion substitution in CeO_2 enhanced oxygen storage capacity, a property required for the easy extraction of lattice oxygen by CO to CO_2 [23–26]. There are a number of studies on CO oxidation and WGS reactions over Fe_2O_3-CeO_2 [27], Au/FeO_x/CeO_2 [28] and Au/CeO_2-Fe_2O_3 [29] catalysts.

Iron (Fe) is a cheaper metal that can be substituted to the extent of 40% in CeO_2 forming a $Ce_{1-x}Fe_xO_{2-\delta}$ solid solution [30]. The Fe^{3+} ion gets reduced only up to the Fe^{2+} state in CeO_2. Fajan's ratio of the Fe^{3+} ion is 44 which is higher than that of the Ce^{4+} ion. $Ce_{1-x}Fe_xO_{2-\delta}$ showed much higher oxygen storage capacity compared to CeO_2. Being a 3d metal ion, the Fe ion has sufficient CO adsorption propensities and therefore, $Ce_{1-x}Fe_xO_{2-\delta}$ can be a good WGS catalyst without any noble metal. If the Pt^{2+} ion is substituted in $Ce_{1-x}Fe_xO_{2-\delta}$, an additional CO adsorption site can be created in addition to enhancing the oxygen storage capacity by synergistic redox interaction between Ce^{4+}/Ce^{3+}, Fe^{3+}/Fe^{2+} and $Pt^{4+}/Pt^{2+}/Pt^0$. Therefore Pt ion substituted $Ce_{1-x}Fe_xO_{2-\delta}$ can be a good WGS catalyst. Indeed, here we report non-deactivating $Ce_{0.67}Fe_{0.33}O_{2-\delta}$ and $Ce_{0.65}Fe_{0.33}Pt_{0.02}O_{2-\delta}$ WGS catalysts.

2. Experimental

2.1. Catalyst preparation and characterization

$Ce_{0.67}Fe_{0.33}O_{2-\delta}$ and $Ce_{0.65}Fe_{0.33}Pt_{0.02}O_{2-\delta}$ solid solutions were synthesized by the sonication method from the starting materials,

* Corresponding author. Tel.: +91 80 2293 2614; fax: +91 80 2360310.
E-mail address: mshegde@sscu.iisc.ernet.in (M.S. Hegde).

0926-3373/$ – see front matter © 2011 Elsevier B.V. All rights reserved.
doi:10.1016/j.apcatb.2011.08.016

$(NH_4)_2Ce(NO_3)_6$ (CAN), $Fe(NO_3)_3{\cdot}9H_2O$, H_2PtCl_6 and diethylenetriamine (DETA) ($C_4H_{13}N_3$) by taking them in the required molar ratio. For the synthesis of $Ce_{0.67}Fe_{0.33}O_{2-\delta}$, 6.7 mmol of CAN is dissolved in 20 ml of distilled water and 3.3 mmol $Fe(NO_3)_3{\cdot}9H_2O$ was dissolved in 5 ml of water. 30 mmol (3.4 ml) of DETA was added to the clear solution containing Ce^{4+} and Fe^{3+} ions. The solution turned into a brown-colored gel immediately. The gel was kept under sonication (Oskar O U 9 equipped with a high intensity piezoelectric resonator, 30 kHz, 100 W cm^{-2}) for 8 h. The temperature of the solution reached up to ~80 °C during sonication. The brown colored precipitate was filtered, washed in hot distilled water and dried in a hot air oven at 110 °C for 3 h. Similarly, for the preparation of $Ce_{0.65}Fe_{0.33}Pt_{0.02}O_{2-\delta}$, 6.5 mmol of CAN and 0.2 mmol of H_2PtCl_6 were dissolved in 20 ml of distilled water and 3.3 mmol of $Fe(NO_3)_3{\cdot}9H_2O$ was dissolved in 5 ml of water. 30 mmol or 3.4 ml of DETA was added. The resulting gel after DETA addition was kept under sonication for 8 h. The solid obtained after filtration and drying at 110 °C for 3 h was brown in color. The dried sample at 110 °C for 3 h was used in all catalytic studies without any pretreatment. A 2 atom% Pt metal impregnated on a $Ce_{0.67}Fe_{0.33}O_{2-\delta}$ catalyst was also prepared by reducing the H_2PtCl_6 solution by hydrazine hydrate (98%, Sigma–Aldrich) over $Ce_{0.67}Fe_{0.33}O_{2-\delta}$ nanocrystallites made by the sonication method. For this purpose 1 g of $Ce_{0.67}Fe_{0.33}O_{2-\delta}$ powder was mixed in 50 ml of distilled water. 0.073 g of H_2PtCl_6 was added to the mixture and stirred for 10 min. Slowly, a hydrazine hydrate solution was added drop by drop to the mixture to reduce the Pt^{4+} ion in H_2PtCl_6 to Pt metal. The mixture was stirred for a further 30 min. The black-colored mixture was filtered and dried at 110 °C for 5 h. The resulting dried solid was further reduced in H_2 at 200 °C.

Powder X-ray diffraction (XRD) patterns are recorded in a Phillips X'Pert diffractometer using Cu-Kα radiation at a scan rate of 0.2° min^{-1} with 0.01° step size in the 2θ range between 10 and 90°. Cu-Kβ radiation was filtered with a graphite crystal post monochromator. The structures of the catalysts were refined by the Rietveld method, using the FullProf-fp2k program [31]. For transmission electron microscopy (TEM) images, a toluene dispersion of the sample was dropped onto the carbon coated Cu grids and the images were recorded with FEI Technai 20 at 200 kV. An EDX analysis was also carried out on the high resolution image in the TEM instrument. X-ray photo-electron spectra (XPS) of selected samples were recorded in a Thermo Scientific Multilab 2000 instrument using Al-Ka at 150 W. The binding energies reported here are with reference to C(1 s) at 284.5 eV and are accurate within ±0.1 eV.

2.2. OSC, CO oxidation and WGS study

The dried samples at 110 °C at 3 h were directly tested in all catalytic studies without any pretreatment. For all the catalytic reactions, the powder catalyst was made into pressed granules of 40–80 mesh sizes and loaded in a micro reactor of length 30 and 0.4 cm of internal diameter. Reactions were carried out as a function of temperature. The oxygen storage/release properties of $Ce_{0.67}Fe_{0.33}O_{2-\delta}$ and $Ce_{0.65}Fe_{0.33}Pt_{0.02}O_{2-\delta}$ were studied by hydrogen uptake measurements carried out over 50 mg of catalyst in a micro reactor with 5.49% H_2/Ar (Chemix, Bangalore, India) at 30 sccm flow rate, up to the temperature of 550 °C. The heating rate was 10 °C min^{-1}. The amount of H_2 consumption or equivalent [O] release was calibrated against hydrogen intake/consumption against the known weight of CuO. Calibrated 10% CO/N_2, 10% O_2/N_2, ultra high pure (UHP) N_2, (UHP) H_2, and UHP CO_2 (Chemix, Bangalore India) were used for CO oxidation and WGS reactions. Direct CO oxidation from the materials was investigated in a micro reactor employing 2 vol% CO balanced in N_2 with a total gas flow of 100 sccm over 200 mg of oxide samples, at a linear heating rate of 10 °C min^{-1} up to 600 °C. CO oxidation over 200 mg of the catalyst at a gas space hourly velocity (GSHV) of 43,000 cm^3 h^{-1} with 2:2 vol% of CO and O_2 with a linear heating rate of 10 °C min^{-1} was carried out. To get the rate of the reaction and activation energy, reactions were carried out by varying the weight of the catalysts ranging from 25 to 200 mg keeping the total gas flow and GSHV same as the above, keeping the catalyst bed length the same and adding the required amount of dilutant namely silica granules of 40–80 mesh sizes.

For the WGS study, 5 cm^3/min CO and 30 cm^3/min H_2O vapor were passed along with N_2 keeping the total gas flow at 130 cm^3/min over 200 mg of catalyst to achieve a GSHV of 55,900 h^{-1}. The ratios of CO:H_2O varied from 1:2, 1:4, 1:6 and 1:8, and the 1:6 ratio was found to be enough to achieve the highest CO conversion. The water vapor in the output gas stream was first condensed before passing to a GC for analysis. The gaseous products obtained from the CO oxidation and WGS reactions were analyzed by an online gas chromatograph (GC). In a GC, N_2 was used as a carrier gas. CO, CO_2 and hydrocarbons were detected by a flame ionization detector (FID). H_2 was detected by a thermal conductivity detector (TCD). The volume of CO, CO_2, H_2 and other byproducts of the reaction (CH_4, other hydrocarbons, HCHO, HCOOH and CH_3OH) were measured independently in a GC in the product stream. To get the rate and activation energy of the reactions, they were carried out by varying the weight of the catalysts from 25 to 200 mg and keeping the total gas flow and GSHV the same.

3. Results and discussion

3.1. Structural analysis

The substitution of 33% Fe^{3+} ions in CeO_2 ($Ce_{0.67}Fe_{0.33}O_{2-\delta}$) and the simultaneous substitution of Pd^{2+} and Fe^{3+} ions in CeO_2 ($Ce_{0.65}Fe_{0.33}Pd_{0.02}O_{2-\delta}$) by the sonochemical method was discussed in our earlier work [30]. In this study, structural analysis is mainly focused on the $Ce_{0.65}Fe_{0.33}Pt_{0.02}O_{2-\delta}$ catalyst. The catalytic activity of both $Ce_{0.67}Fe_{0.33}O_{2-\delta}$ and $Ce_{0.65}Fe_{0.33}Pt_{0.02}O_{2-\delta}$ compounds has been reported here. By the sonication method using DETA as a complexing agent, the simultaneous substitution of such a high proportion of Fe^{3+} ion along with Pt^{4+} ions in the CeO_2 lattice was achieved after 8 h of sonication with the quantitative precipitation of $Ce_{0.65}Fe_{0.33}Pt_{0.02}O_{2-\delta}$. Rietveld-refined powder XRD patterns of $Ce_{0.67}Fe_{0.33}O_{2-\delta}$ and $Ce_{0.65}Fe_{0.33}Pt_{0.02}O_{2-\delta}$ are shown in Fig. 1(a) and (b) respectively. Both the compounds crystallize in a fluorite structure. All the peaks were indexed to a cubic fluorite structure (space group: $Fm3m$) and no diffraction lines were found due to Fe–DETA, Pt–DETA complexes, Fe_2O_3, Fe_3O_4, FeO, Pt, PtO and PtO_2 in powder XRD patterns. The lattice parameters of $Ce_{0.67}Fe_{0.33}O_{2-\delta}$ and $Ce_{0.65}Fe_{0.33}Pt_{0.02}O_{2-\delta}$ are found to be 5.341(2) Å and 5.357(3) Å respectively, and are much smaller compared to the lattice parameter of CeO_2 (5.411 Å) (JCPDS No.: 340394). A decrease in the lattice parameter of $Ce_{0.67}Fe_{0.33}O_{2-\delta}$ and $Ce_{0.65}Fe_{0.33}Pt_{0.02}O_{2-\delta}$ also confirms the substitution of smaller Fe^{3+} and Pt^{4+} ions for bigger Ce^{4+} ions in the CeO_2 lattice. The XRD profiles fit well with the observed XRD data. The observed XRD peaks are broad suggesting that the crystallites are nanometer in size and the average crystallite size was estimated by following the Scherrer formula [32]:

$$\text{Crystallites size}(d) = \frac{0.9\lambda}{\beta \cos\theta} \quad (1)$$

where λ is the wavelength of the X-ray, β is the full width at half maxima (FWHM) in the radian and θ is the diffraction angle. FWHM was estimated by the equation [33],

$$\beta = (U \tan^2\theta + V \tan\theta + W)^{1/2} \quad (2)$$

Table 1
Structural parameters of the catalysts.

Compound	Lattice parameter (a)	R_{bragg}	R_f	χ^2
$Ce_{0.67}Fe_{0.33}O_{2-\delta}$ (as prepared)	5.341(1)	0.75	0.49	1.41
$Ce_{0.65}Fe_{0.33}Pt_{0.02}O_{2-\delta}$ (as prepared)	5.357(1)	0.71	0.57	1.32
$Ce_{0.65}Fe_{0.33}Pt_{0.02}O_{2-\delta}$ (spent catalyst after 10 cycles of WGS reaction)	5.399(1)	0.85	0.58	1.12

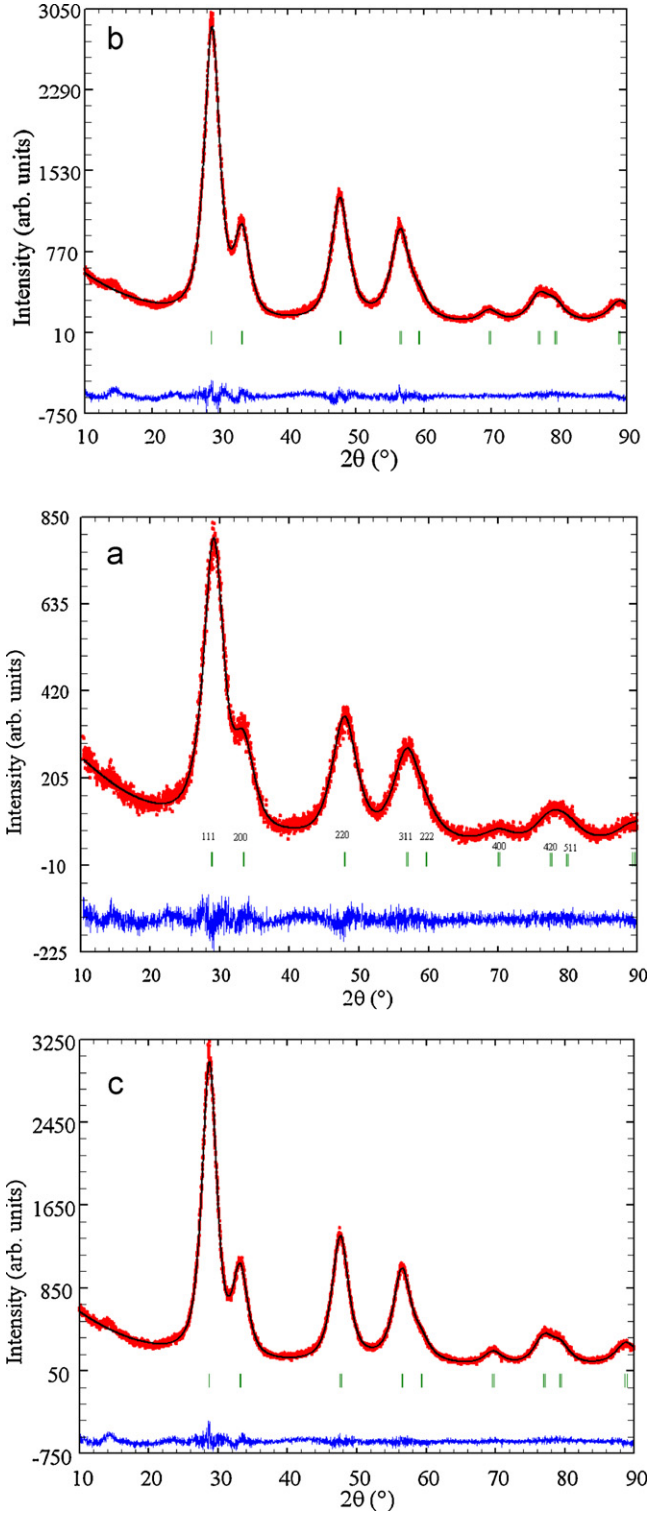

Fig. 1. Rietveld refined powder XRD profile of (a) $Ce_{0.67}Fe_{0.33}O_{2-\delta}$, (b) $Ce_{0.65}Fe_{0.33}Pt_{0.02}O_{2-\delta}$, and (c) $Ce_{0.65}Fe_{0.33}Pt_{0.02}O_{2-\delta}$ after 10 cycles of WGS reactions.

By taking the U, V, W values from the Rietveld refinement data for (1 1 1), (2 0 0), (2 2 0) and (3 1 1) diffraction lines, the crystallite sizes are found to be in the range of 3–5 nm. Crystallite sizes and structural parameters R_f, R_{bragg}, and χ^2 obtained from the Rietveld refinement of powder XRD data of $Ce_{0.67}Fe_{0.33}O_{2-\delta}$ and $Ce_{0.65}Fe_{0.33}Pt_{0.02}O_{2-\delta}$ are summarized in Table 1.

Bright field and HRTEM images of $Ce_{0.675}Fe_{0.33}Pt_{0.02}O_{2-\delta}$ are shown in Fig. 2(a) and (b). Electron diffraction patterns and an enlarged view of lattice fringes are shown in the inset of Fig. 2(a) and (b) respectively. A ring pattern is assigned to the fluorite structure and the width of the lattice fringes are 3.11 Å which agrees well with the d_{111} planes of the fluorite $Ce_{0.67}Fe_{0.33}Pt_{0.02}O_{2-\delta}$ lattice. The absence of diffraction lines and lattice fringes due to any iron oxide such as Fe_2O_3, Fe_3O_4, FeO and Pt-oxide such as PtO and PtO_2 phases suggests that Fe and Pt are substituted in a ceria lattice. The bright field image and the HRTEM image showed that individual crystallites sizes are 3–4 nm and are well connected with each other. Crystallite sizes from the TEM study agree well with the XRD study.

The oxidation state of the metal ions present in $Ce_{0.67}Fe_{0.33}O_{2-\delta}$ and $Ce_{0.65}Fe_{0.33}Pt_{0.02}O_{2-\delta}$ was investigated by X-ray photoelectron spectroscopy. The core level Fe(2p) spectra of $Ce_{0.67}Fe_{0.33}O_{2-\delta}$ and $Ce_{0.65}Fe_{0.33}Pt_{0.02}O_{2-\delta}$ are shown in Fig. 3(a) and (b) respectively. The binding energy of Fe($2p_{3/2}$) is observed at 710.4 eV and a weak satellite at 8 eV from the main peak confirms Fe in the 3+ state in both the compounds [34]. Thus Fe is in 3+ state is also shown by Mossbauer spectroscopy [29]. The Ce(3d) spectra of $Ce_{0.67}Fe_{0.33}O_{2-\delta}$ and $Ce_{0.65}Fe_{0.33}Pt_{0.02}O_{2-\delta}$ are shown in Fig. 4(a) and (b). The Ce($3d_{5/2}$) peak was observed at 882.7 eV along with satellite peaks at 6.4 and 16 eV from the main peak, which are characteristic peaks of Ce^{4+} in CeO_2. Ce^{3+}(3d) in Ce_2O_3 is characterized by Ce($3d_{5/2}$) at 883.3 eV along with an intense satellite at 887.1 eV [35]. In the as prepared $Ce_{0.67}Fe_{0.33}O_{2-\delta}$, Ce seems to be mostly in 4+ state as can be seen from Fig. 4(a). Small % of Ce in 3+ state with the extent of 1–3% is difficult to detect by XPS. A partial filling of the valley between Ce^{4+}($3d_{5/2}$) at 882.7 eV and its satellite at 889.1 eV (Fig. 4(b)) confirms that Ce is in mixed valent (4+, 3+) states in $Ce_{0.65}Fe_{0.33}Pt_{0.02}O_{2-\delta}$. Therefore, the Ce(3d) spectrum was resolved into it Ce^{3+} and Ce^{4+} components. It is found that in $Ce_{0.65}Fe_{0.33}Pt_{0.02}O_{2-\delta}$, ~10% of Ce is present in the 3+ state. The core level Pt(4f) spectra of $Ce_{0.65}Fe_{0.33}Pt_{0.02}O_{2-\delta}$ is shown in Fig. 5(a). The binding energy of Pt($4f_{7/2}$) was observed at 74.3 eV. The binding energy of Pt^{4+}($4f_{7/2}$) in PtO_2 is observed at 74.3 eV [36]. So Pt is in the 4+ oxidation state in the as-prepared $Ce_{0.65}Fe_{0.33}Pt_{0.02}O_{2-\delta}$. Therefore, the formula of $Ce_{0.65}Fe_{0.33}Pt_{0.02}O_{2-\delta}$ can be written as $Ce_{0.55}{}^{4+}Ce_{0.10}{}^{3+}Fe_{0.33}{}^{3+}Pt_{0.02}{}^{2+}O_{1.785}$ and $Ce_{0.67}Fe_{0.33}O_{2-\delta}$ can be written as $Ce_{0.67}{}^{4+}Fe_{0.33}{}^{3+}O_{1.835}$.

An Estimation of the relative surface concentrations of Ce and Fe and Ce:Fe:Pt was carried out from the intensities of Fe(2p) and Ce(3d) and Pt(4f) peaks in $Ce_{0.67}Fe_{0.33}O_{2-\delta}$ and $Ce_{0.65}Fe_{0.33}Pt_{0.02}O_{2-\delta}$. The relative surface concentration is calculated from the formula [37]

$$\text{Relative concentration, } C_M = \frac{I_M/\lambda_M\sigma_M D_M}{\sum(I_M/\lambda_M\sigma_M D_M)} \quad (3)$$

where I_M is the integrated intensity of the core levels (M = Ce(3d), Fe(2p) and Pt(4f)), λ_M is the mean escape depths of the respective photoelectrons, σ_M is the photoionization cross-section, and D_M

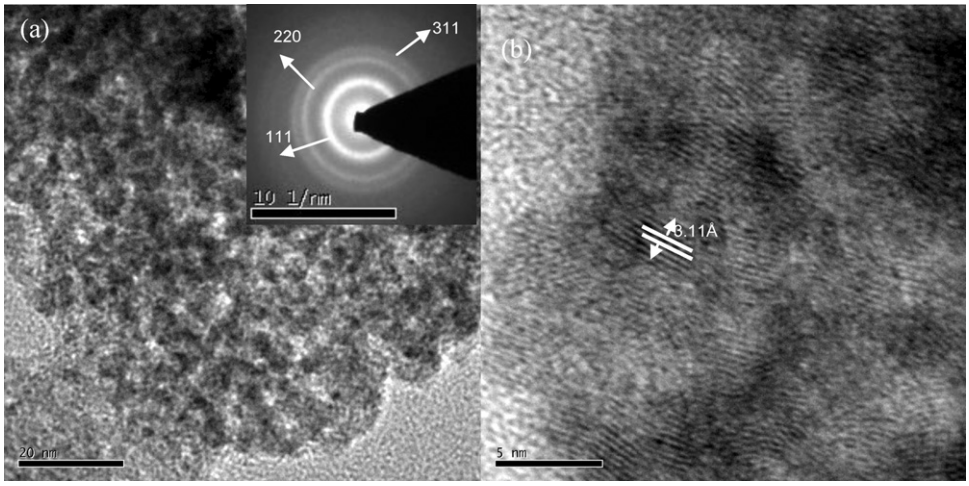

Fig. 2. (a) Bright filed image of $Ce_{0.65}Fe_{0.33}Pt_{0.02}O_{2-\delta}$ and electron diffraction in the inset; (b) HRTEM image of $Ce_{0.65}Fe_{0.33}Pt_{0.02}O_{2-\delta}$.

is the geometric factor. The photoionization cross-section values were taken from Scofield's data [38] and the mean escape depths were taken from Penn's data [39]. The geometric factor was taken as 1 because the maximum intensity in this spectrometer is obtained at 90°. The surface concentrations of Ce, Fe and Pt were found in the ratio of 0.66:0.31:0.03 in $Ce_{0.65}Fe_{0.33}Pt_{0.02}O_{2-\delta}$. Thus, the surface composition of $Ce_{0.67}Fe_{0.33}O_{2-\delta}$ and $Ce_{0.65}Fe_{0.33}Pt_{0.02}O_{2-\delta}$ are almost the same as the bulk composition takes in the preparation.

3.2. Oxygen storage capacity (OSC)

To see the effect of Fe^{3+} and Pt^{4+} ion substitution on the OSC of CeO_2, hydrogen uptake measurements were carried out. The hydrogen uptake plots for (a) CeO_2, (b) $Ce_{0.67}Fe_{0.33}O_{2-\delta}$ and (c) $Ce_{0.65}Fe_{0.33}Pt_{0.02}O_{2-\delta}$ are given in Fig. 6. $Ce_{0.65}Fe_{0.33}Pt_{0.02}O_{2-\delta}$ showed a very sharp hydrogen reduction/uptake at ~80 °C. However, broad peaks were observed for $Ce_{0.67}Fe_{0.33}O_{2-\delta}$ at a temperature range of 200–450 °C. Pure CeO_2 (4–5 nm sizes) made by the same sonication method showed a reduction of 0.14 [O]/mol of the compound and $Ce_{0.67}Fe_{0.33}O_{2-\delta}$ showed a reduction of 0.28 [O]/mol of the compound up to 500 °C. $Ce_{0.65}Fe_{0.33}Pt_{0.02}O_{2-\delta}$ showed hydrogen a uptake/reduction of 0.14 [O]/mol of the compound up to 150 °C and 0.32 [O]/mol of the compound up to 500 °C. Thus, a much higher reduction is observed at lower temperatures in the case of $Ce_{0.65}Fe_{0.33}Pt_{0.02}O_{2-\delta}$ compared to $Ce_{0.67}Fe_{0.33}O_{2-\delta}$ and CeO_2. If only Pt^{4+} had been reduced to the Pt^0 state, the H_2/Pt ratio should have been 2 but the H_2/Pt ratio was found to be 7 (≤150 °C).

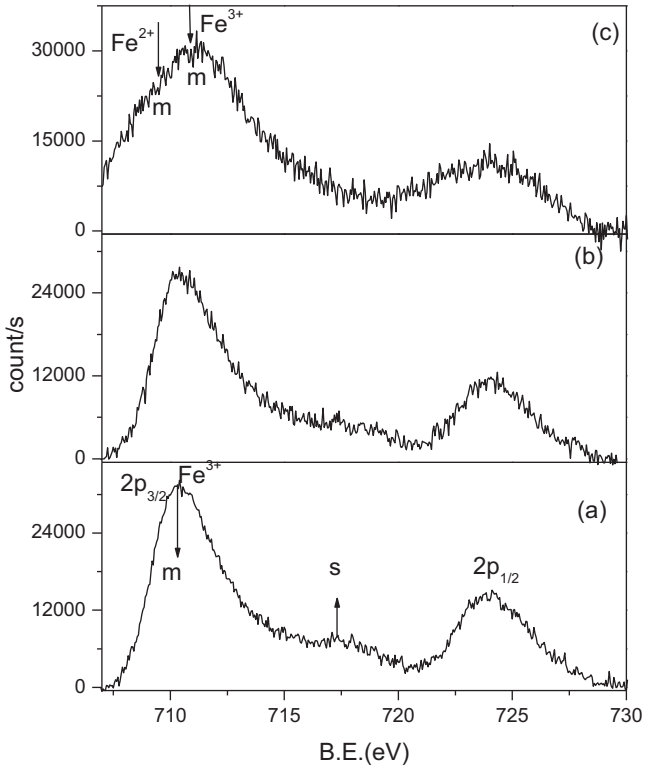

Fig. 3. Core level Fe(2p) XPS of (a) $Ce_{0.67}Fe_{0.33}O_{2-\delta}$, (b) $Ce_{0.65}Fe_{0.33}Pt_{0.02}O_{2-\delta}$ (as prepared) and (c) $Ce_{0.65}Fe_{0.33}Pt_{0.02}O_{2-\delta}$ after 10 cycles of WGS reactions.

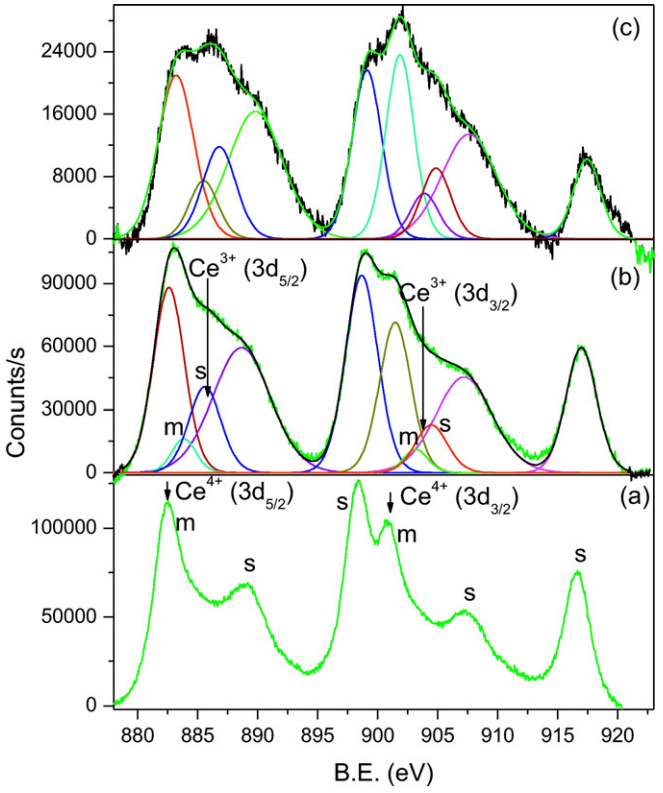

Fig. 4. Core level Ce(3d) XPS of (a) $Ce_{0.67}Fe_{0.33}O_{2-\delta}$, (b) $Ce_{0.65}Fe_{0.33}Pt_{0.02}O_{2-\delta}$ (as prepared) and (c) $Ce_{0.65}Fe_{0.33}Pt_{0.02}O_{2-\delta}$ after 10 cycles of WGS reactions.

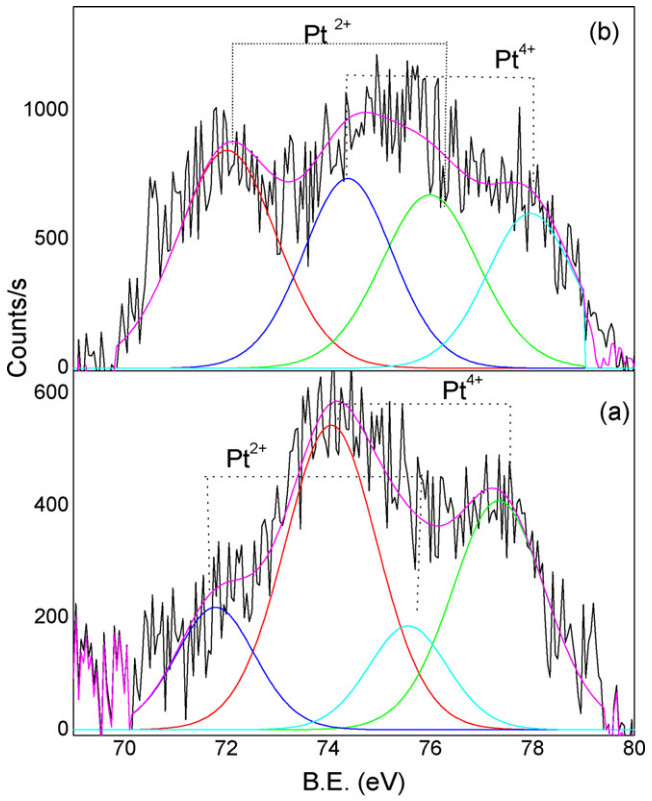

Fig. 5. Core level Pt(4f) XPS of (a) $Ce_{0.65}Fe_{0.33}Pt_{0.02}O_{2-\delta}$ and (b) $Ce_{0.65}Fe_{0.33}Pt_{0.02}O_{2-\delta}$ after 10 cycles of WGS reactions.

This higher H_2/Pt ratio can be assigned to a hydrogen spillover from Pt^{4+} ions to neighboring Fe^{3+} and Ce^{4+} ions. The enhanced storage of H_2 over Pt^{2+} ions or the hydrogen spillover from Pt ions to the Ce^{4+} ion in $Ce_{1-x}Pt_xO_{2-\delta}$ has been discussed in our earlier study [40,41].

3.3. CO oxidation study

%CO oxidation to CO_2 over $Ce_{0.67}Fe_{0.33}O_{2-\delta}$ and $Ce_{0.65}Fe_{0.33}Pt_{0.02}O_{2-\delta}$ catalysts in the presence and absence of oxygen are shown in Fig. 7. CO conversion in the absence of feed oxygen was observed in a broad temperature range (150–550 °C) in the case of $Ce_{0.67}Fe_{0.33}O_{1.835}$. The complete conversion of CO to CO_2 was achieved at below 125 °C for $Ce_{0.65}Fe_{0.33}Pt_{0.02}O_{1.785}$

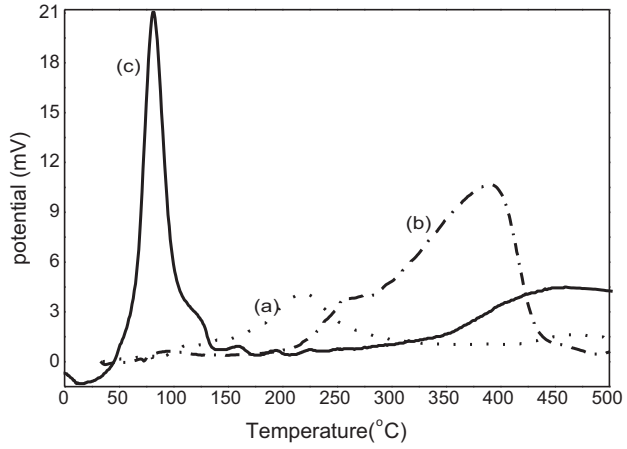

Fig. 6. Hydrogen uptake plot for (a) CeO_2, (b) $Ce_{0.67}Fe_{0.33}O_{2-\delta}$ and (c) $Ce_{0.65}Fe_{0.33}Pt_{0.02}O_{2-\delta}$.

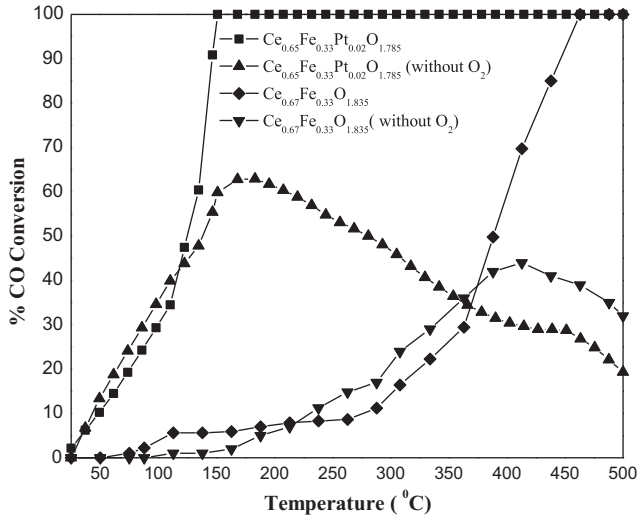

Fig. 7. CO oxidation plot with $Ce_{0.65}Fe_{0.33}Pt_{0.02}O_{2-\delta}$ (a) with feed oxygen, (b) in the absence of feed oxygen and with $Ce_{0.67}Fe_{0.33}O_{2-\delta}$ (c) with feed oxygen and (d) in the absence of feed oxygen.

and 450 °C for $Ce_{0.67}Fe_{0.33}O_{1.835}$ in the presence of feed oxygen. Due to the substitution of 2 atom% Pt ion in $Ce_{0.67}Fe_{0.33}O_{1.835}$, $Ce_{0.65}Fe_{0.33}Pt_{0.02}O_{1.785}$ showed much higher activity for CO oxidation. In the case of $Ce_{0.65}Fe_{0.33}Pt_{0.02}O_{1.785}$, high CO conversion is observed at a lower temperature with a reduction peak around 170 °C indicating higher lattice oxygen extraction by CO. Thus feed O_2 can be reversibly exchanged with lattice oxygen in $Ce_{0.65}Fe_{0.33}Pt_{0.02}O_{1.785}$ and due to this exchange, highly active for CO oxidation was obtained with this catalyst.

To derive the rate and activation energy of the catalysts for CO oxidation, experiment were carried out with different weights of the catalyst keeping the total gas flow and GHSV at 43,000 h^{-1}. The rate was determined using the following equation:

$$\text{Rate}(r) = \frac{F \times x}{W} = \frac{x}{W/F} \quad (4)$$

where F is the flow of the gas in cm^3/s, W is the weight of the catalyst in g and x is the fractional conversion. The fraction conversion (x) vs. the W/F plot for the $Ce_{0.67}Fe_{0.33}O_{1.835}$ catalyst is shown in Fig. 8(a) and the rate (r) vs. T (°C) is given in Fig. 8(b). The fractional conversion (x) vs. the W/F plot is linear up to 70% conversion. ln(r) vs. 1000/T (K^{-1}) is given in the inset of Fig. 8(b). The activation energy is calculated from the slope of ln(r) vs. 1000/T (K^{-1}) plot. Even in the absence of any noble metal, $Ce_{0.67}Fe_{0.33}O_{1.835}$ acts as a good catalyst for CO oxidation and the rate is 1.3 μmol g^{-1} s^{-1} at 450 °C and the activation energy is 56.3 kJ mol^{-1}.

The fraction conversion (x) vs. the W/F plot for the $Ce_{0.65}Fe_{0.33}Pt_{0.02}O_{1.785}$ catalyst is shown in Fig. 9(a) and the rate (r) vs. T (°C) is given in Fig. 9(b). The W/F plot is a liner up to 75% conversion. ln(r) vs. 1000/T (K^{-1}) is also linear as shown in the inset of Fig. 8(b). The activation energy from the plot is found to be15.2 kJ mol^{-1} and the rate is 2 μmol g^{-1} s^{-1} at 100 °C, Pt ion substitution enhances CO oxidation activity to a large extent. Thus Pt ion substituted $Ce_{0.67}Fe_{0.33}O_{2-\delta}$ is an excellent CO oxidation catalyst.

3.4. WGS study

In Fig. 10(a), % concentrations of CO, CO_2 and H_2 as a function of temperature are plotted for the $Ce_{0.67}Fe_{0.33}O_{1.835}$ catalyst. Near-complete CO conversion to CO_2 and H_2 was observed at 450 °C and even at higher temperatures (up to 550 °C) no decrease in conversion is observed with $Ce_{0.67}Fe_{0.33}O_{1.835}$. In Fig. 10(b), %

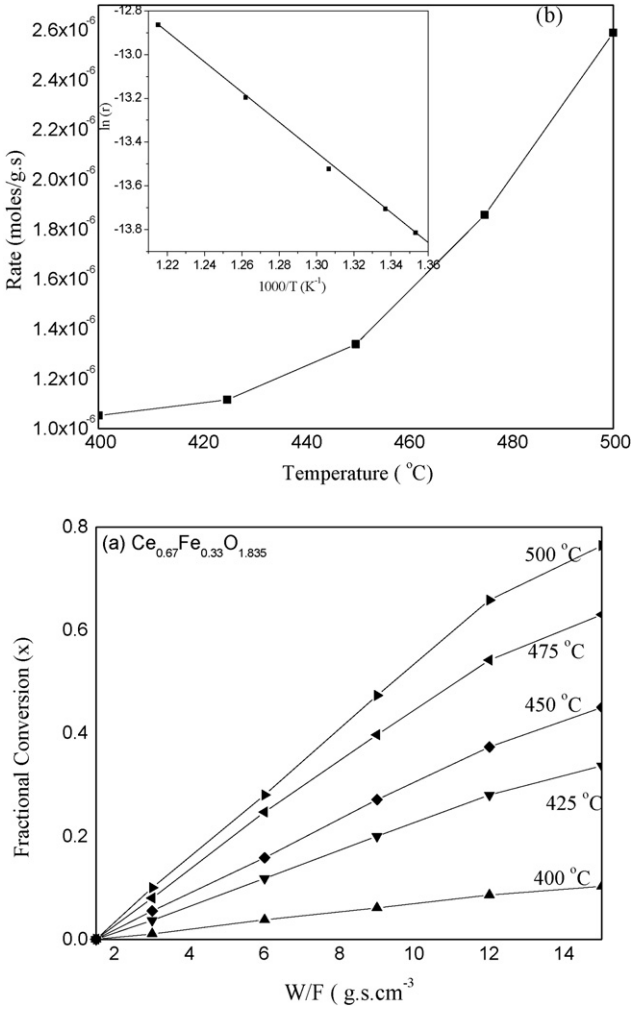

Fig. 8. (a) Fractional conversion vs. (W/F), (b) rate (r) vs. temperature (°C) and ln(r) vs. 1000/T (K^{-1}) for CO oxidation with $Ce_{0.67}Fe_{0.33}O_{2-\delta}$ catalyst.

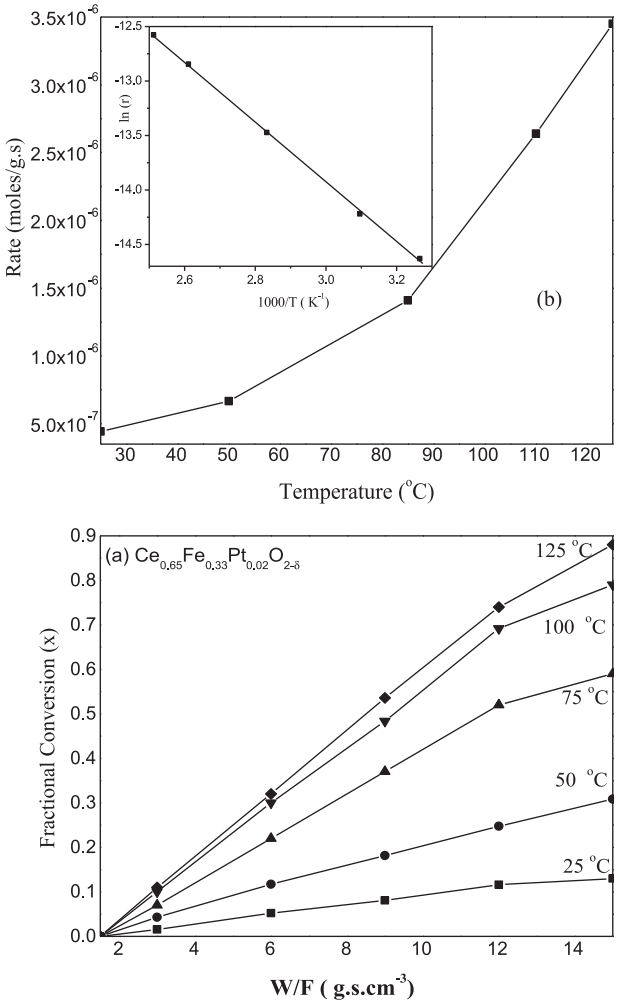

Fig. 9. (a) Fractional conversion vs. (W/F), (b) rate (r) vs. temperature (°C) and ln(r) vs. 1000/T (K^{-1}) for CO oxidation with $Ce_{0.65}Fe_{0.33}Pt_{0.02}O_{2-\delta}$ catalyst.

concentrations of CO, CO_2 and H_2 as a function of temperature are plotted for the $Ce_{0.65}Fe_{0.33}Pt_{0.02}O_{1.785}$ catalyst. Complete CO conversion to CO_2 and H_2 was observed at 285 °C and even at higher temperatures (up to 550 °C) no decrease in conversion was observed. Possible byproducts of the reaction such as CH_3OH, H_2CO, CH_4, and other hydrocarbons were not detected in the product stream in the detection limit of 5 ppm. CO conversion is almost 100% H_2 specific with both the catalysts.

The WGS reaction is considered to be an equilibrium reaction:

$$CO + H_2O \rightarrow CO_2 + H_2 \quad (5)$$

However the reaction seems to takes place in steps

$$CO + [O]_x \rightarrow CO_2 + V_O^{2-}; \quad (6)$$

$$V_O^{2-} + H_2O \rightarrow [O]_x + H_2 \quad (7)$$

Here $[O]_x$ indicates oxygen occupied in the lattice and V_O^{2-} indicates oxide vacancy. Indeed, the $Ce_{0.65}Fe_{0.33}Pt_{0.02}O_{1.785}$ catalyst showed much higher CO oxidation activity both in the presence and absence of feed oxygen. So in the first step of the WGS reaction, CO is oxidized to CO_2 by lattice oxygen. The reaction can be written as follows:

$$Ce_{0.65}Fe_{0.33}Pt_{0.02}O_{1.785} + \delta CO \rightarrow Ce_{0.65}Fe_{0.33}Pt_{0.02}O_{1.785-\delta} + \delta CO_2. \quad (8)$$

This step creates additional oxide ion vacancies in the catalyst lattice. H_2O can be adsorbed on vacant lattice oxygen sites. The catalyst lattice is regenerated by releasing hydrogen.

$$Ce_{0.65}Fe_{0.33}Pt_{0.02}O_{1.785-\delta} + \delta H_2O \rightarrow Ce_{0.65}Fe_{0.33}Pt_{0.02}O_{1.785} + \delta H_2 \quad (9)$$

To confirm the sequence of the reactions above, first CO was passed over 200 mg of the catalyst at 250 °C for 20 min. CO_2 via utilization of lattice oxygen was observed in the out put stream. H_2O vapor with N_2 was passed over the catalyst at the same temperature and H_2 generation was indeed observed proving the WGS mechanism by Eqs. (8) and (9).

Almost complete conversion (>99%) of CO to CO_2 with 100% H_2 selectivity was observed with the $Ce_{0.65}Fe_{0.33}Pt_{0.02}O_{1.785}$ catalyst in the temperature range of 285–550 °C. Pt free $Ce_{0.67}Fe_{0.33}O_{2-\delta}$ also is a good WGS catalyst but works at a higher temperature. Taking in to account that WGS is an equilibrium reaction, an equilibrium constant can be obtained from the Moe equation [42]:

$$\text{Equilibrium constant, } K_{eq} = \exp\left(\frac{4577.8}{T} - 4.33\right) \quad (10)$$

By taking the input gas composition of our experiment in Eq. (10), equilibrium conversion is >94% at 500 °C. Equilibrium conversion for the WGS reaction is plotted (dotted line) in Fig. 10(a) and (b). However, nearly complete conversion (~99%) of CO to CO_2 and H_2 was observed with the catalyst even up to 550 °C. Equilibrium

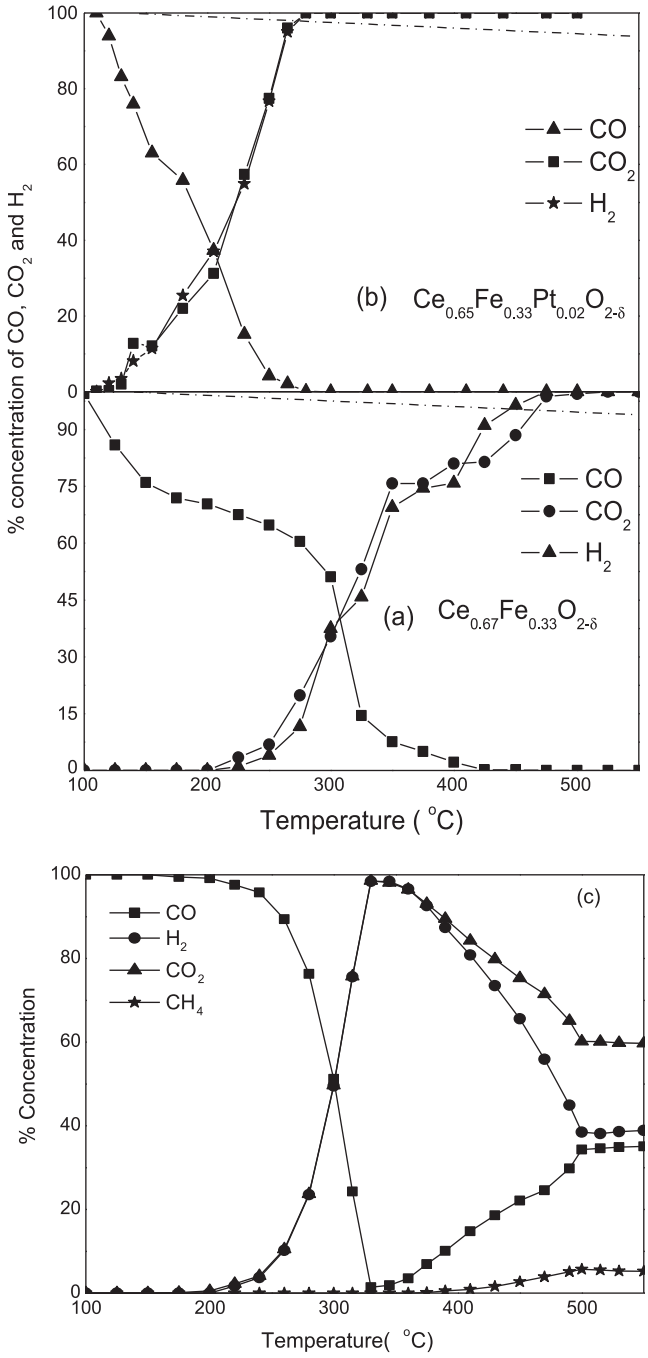

Fig. 10. (a) % CO, CO_2 and H_2 concentrations in WGS reactions (gas composition: 2 cm^3/min CO, 30 cm^3/min H_2O balance with N_2 keeping total gas flow 130 cm^3/min) with (a) $Ce_{0.67}Fe_{0.33}O_{2-\delta}$ (b) $Ce_{0.65}Fe_{0.33}Pt_{0.02}O_{2-\delta}$ and (c) 2 atom% Pt impregnated on $Ce_{0.67}Fe_{0.33}O_{2-\delta}$. (*Note*: Equilibrium CO_2 formation or CO conversion is plotted by dash-dot line in a and b.)

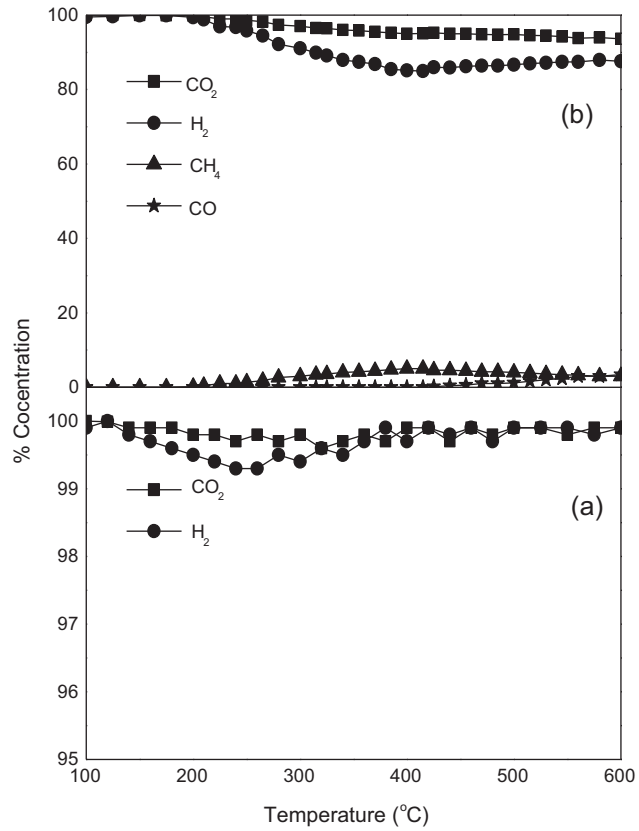

Fig. 11. (a) % CO_2, H_2 and CO concentrations in reverse WGS reactions (gas composition: 2 cm^3/min CO_2 and H_2, 30 cm^3/min H_2O balance with N_2 keeping total gas flow 130 cm^3/min) with $Ce_{0.65}Fe_{0.33}Pt_{0.02}O_{2-\delta}$. (b) % CO_2, H_2 and CO concentrations in reverse WGS reactions (gas composition: 2 cm^3/min CO_2 and H_2, balance with N_2 keeping total gas flow 130 cm^3/min) with $Ce_{0.65}Fe_{0.33}Pt_{0.02}O_{2-\delta}$.

conversion is a thermodynamic phenomenon, but with this catalyst, the operation of the redox mechanism seems to shift the equilibrium to the right side. The shift of equilibrium to the left side should bring down % CO conversion. This can happen if CO_2 and H_2 adsorption are significant for the reverse WGS reaction. The catalyst does not seem to support a reverse WGS reaction.

To prove this, we did a reverse WGS reaction over the $Ce_{0.65}Fe_{0.33}Pt_{0.02}O_{1.785}$ catalyst both in the presence and absence of feed H_2O. First, we did the experiment with gas composition 2 cm^3/min CO_2, 2 cm^3/min H_2 and 30 cm^3/min H_2O balance in N_2 with total flow 130 cm^3/min over 200 mg of the catalyst. % CO_2 and H_2 concentration is shown as function temperature (Fig. 11(a)). CO formation does not occur with the catalyst and there was no measurable decrease in the concentration of H_2 and CO_2 even up to 600 °C. Later, we did the experiment with gas composition 2 cm^3/min CO_2 and 2 cm^3/min H_2 balanced in N_2 with total flow 130 cm^3/min over 200 mg of the catalyst without H_2O in the flow. % CO_2 and H_2 concentration is shown in function temperature (Fig. 11(b)). In the absence of feed H_2O, methane formation was observed above 400 °C in addition to CO formation above 500 °C. Thus, in the presence of excess H_2O in the reaction stream, a reverse WGS reaction is not formed over $Ce_{0.65}Fe_{0.33}Pt_{0.02}O_{1.785}$. This means that in the presence of a high flow of H_2O vapors, CO_2 absorption does not occur over the catalyst and no reverse WGS reaction occurs. However, in the absence of H_2O vapor, a reverse WGS reaction and methane formation were observed. We believe that the lower or almost no absorption of CO_2 over the catalyst in the presence of an excess feed of H_2O vapor is due to the presence of Pt in the ionic state (2+ and 4+) and the Fe^{3+} ion in CeO_2 lattice in this catalyst. As the charge by size ratio of Pt^{4+} is very high compared to Pt^{2+} and Pt metal, according to Fajan's rule the Pt^{4+} ion is much more acidic. That is why the absorption propensity of acidic CO_2 is lower on the Pt ion compared to Pt metal and in the presence of excess water as in the case of a WGS reaction, the reverse reaction $CO_2 + H_2 \rightarrow CO + H_2O$ does not occur.

Further, to prove the point that ionic Pt plays a unique role, we also did the WGS reaction over 2 atom% Pt metal impregnated on the $Ce_{0.67}Fe_{0.33}O_{1.835}$ catalyst. We did the WGS study with gas composition 2 cm^3/min CO and 30 cm^3/min H_2O balance in N_2 with a total flow of 130 cm^3/min over 200 mg of catalyst. % CO conversion and CO_2 and H_2 formation are plotted as functions of temperature

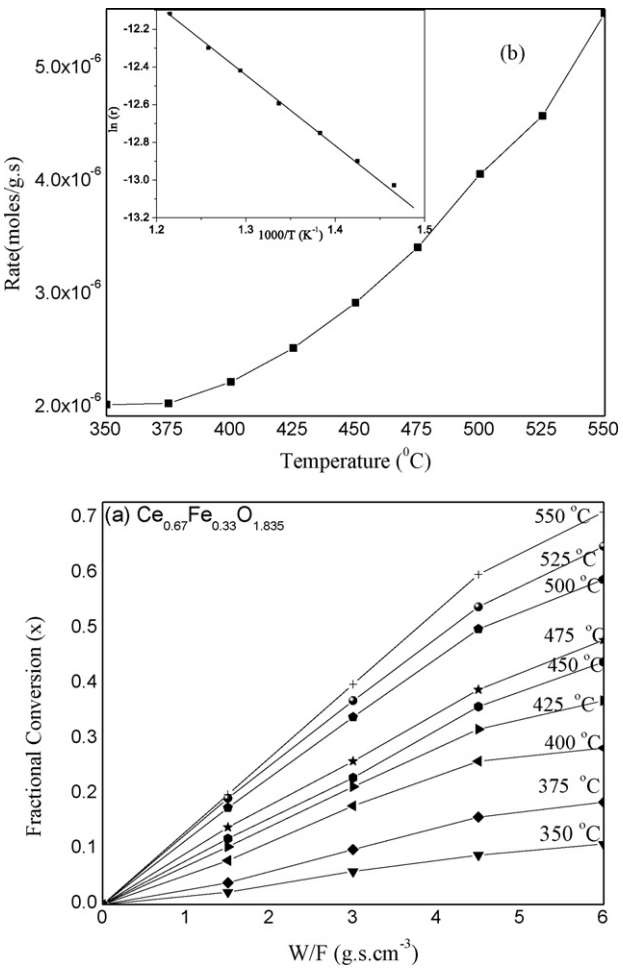

Fig. 12. (a) Fractional conversion vs. (W/F), (b) rate (r) vs. temperature (K) and ln(r) vs. 1000/T (K^{-1}) for H_2 formation in WGS reactions with $Ce_{0.67}Fe_{0.33}O_{2-\delta}$ catalyst.

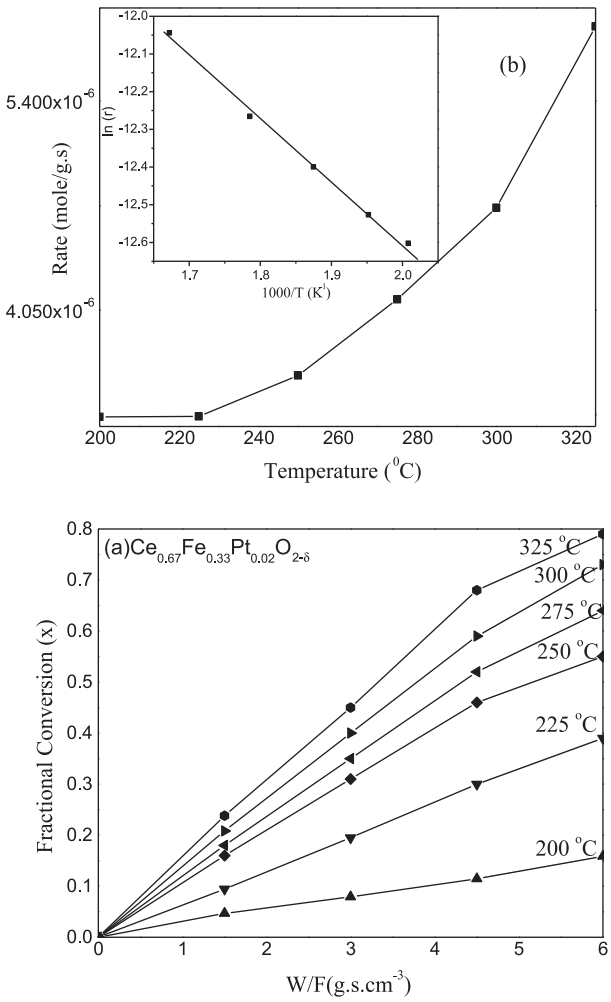

Fig. 13. (a) Fractional conversion vs. (W/F), (b) rate (r) vs. temperature (K) and ln(r) vs. 1000/T (K^{-1}) for H_2 formation in WGS reactions with $Ce_{0.65}Fe_{0.33}Pt_{0.02}O_{2-\delta}$ catalyst.

(Fig. 10(c)). A nearly complete conversion of CO to CO_2 (~99%) was observed around 330 °C and above this temperature CO conversion to CO_2 started decreasing. At 500 °C, only ~60% CO conversion to CO_2 was observed. Methane formation was observed above 375 °C. This means that over the Pt metal impregnated catalyst, CO dissociation leading to CH_4 occurs.

To calculate the rate and activation energy of the catalyst, WGS reactions were carried out with varying amounts of catalyst, keeping the GHSV and total gas flow the same. Fractional conversion (x) vs. W/F plot for the $Ce_{0.67}Fe_{0.33}O_{1.835}$ catalyst is shown in Fig. 12(a) and the rate (r) vs. T (°C) is given in Fig. 12(b). The Fractional conversion (x) vs. the W/F plot is linear up to 60% conversion. ln(r) vs. 1000/T (K^{-1}) is given in the inset of Fig. 12(b). The activation energy was calculated from the slope of ln(r) vs. 1000/T (K^{-1}) plot. $Ce_{0.67}Fe_{0.33}O_{1.835}$ acts as a good WGS catalyst and the rate is found to be 2.8 μmol g^{-1} s^{-1} at 450 °C and the activation energy was found to 33.8 kJ mol^{-1}. Fractional conversion (x) vs. the W/F plot for the $Ce_{0.65}Fe_{0.33}Pt_{0.02}O_{1785}$ catalyst is shown in Fig. 13(a) and the rate (r) vs. T (°C) is given in Fig. 13(b). The Fractional conversion (x) vs. the W/F plot is linear up to 70% conversion. ln(r) vs. 1000/T (K^{-1}) is given in the inset of Fig. 13(b). The rate is found to be as high as 4.05 μmol g^{-1} s^{-1} at 275 °C and the activation energy was found to 12.1 kJ mol^{-1}. A comparison of the rate, TOF and activation energy of different catalysts is given (Table 2). As can be seen from the table that is presented, a Pt free catalyst works well and no noble metal is needed for high conversion. A Pt ion substituted catalyst indeed gives high rates of conversion with low activation energy.

WGS catalysts are used to reform the CO in to H_2; the feed gas comes from the reforming of hydrocarbon containing a higher volume of CO_2 and H_2. Therefore the WGS reaction activity of the catalyst should be examined in the presence of excess H_2 and CO_2. Therefore the WGS reaction was also studied in the presence of excess fed H_2 and CO_2 with a gas mixture flow of CO (2 cm^3/min), CO_2 (10 cm^3/min) and H_2 (10 cm^3/min) balance in N_2, keeping the total gas flow and GSHV the same with 200 mg of catalyst. In Fig. 14, % CO, H_2 and CO_2 concentrations are plotted as a function of temperature. H_2 and CO_2 concentrations are plotted by deducting the input gas amount from the product output. That is why the initial CO_2 and H_2 concentration is zero. Even in the presence of externally fed H_2 and CO_2, almost 99% conversion is observed at 375 °C, and conversion remains high even up to 550 °C. Thus the catalyst was highly active even in the presence of externally fed H_2 and CO_2. Equilibrium conversion is also plotted taking thermodynamic considerations in to account. For the reaction mixture, equilibrium CO conversion to CO_2 or H_2 conversion should be ~90% at 500 °C. Again, equilibrium conversion is less than what is observed experimentally.

A WGS reaction was repeatedly carried out for 10 cycles with gas composition 2 cm^3/min CO, 10 cm^3/min CO_2, 10 cm^3/min H_2 and 30 cm^3/min H_2O vapor balance with N_2. In each cycle, the WGS reaction was started from 100 °C to 500 °C and then kept for 5 h at 500 °C. The reaction was stopped (gas flow was stopped and the

Table 2
Comparison of rate and activation for WGS reactions with different catalysts.

Compound	%CO	%H_2O	%H_2	%CO_2	Max. conversion (%) and T max. (°C)	Rate (μmol g^{-1} s^{-1}) at temp (°C)	Turn over frequency (s^{-1}) at temp (°C)	E_a (kcal/mol)	Reference
0.5%Pt/CeO_2	3	7.5			≥99.5, 300				[43]
0.5% Pt/$Ce_{0.5}Ti_{0.5}O_2$	3	7.5			≥99.5, 300				[43]
0.5%Pt/TiO_2	3	7.5			≥99.5, 300				[43]
1.5%Pt10%La/CeO_2	11	26	26	7	≥99.5	1.0 (350)	0.015 (350)	18	[11]
2.7% Pt10%La/CeO_2	11	26	26	7	≥99.5	1.5 (350)	0.011 (350)	18	[11]
3.7% Pt10%La/CeO_2	11	26	26	7	≥99.5	2 (350)	0.01 (350)	18	[11]
1%Pt/CeO_2	7	22	37	8.5		0.59 (200)	0.01 (200)		[11]
$Ti_{0.99}Pt_{0.01}O_{2-\delta}$	2	30	50		97, 310	12.9 (280)	0.104 (280)	10	[20]
$Ce_{0.78}Ti_{0.20}Pt_{0.02}O_{2-\delta}$	2	30			≥99.8, 360	14.5 (220)	0.109 (220)		[20]
$Ce_{0.78}Ti_{0.20}Pt_{0.02}O_{2-\delta}$	2	30	50		98, 355	7.54 (280)	0.058 (280)	13.5	[20]
$Ce_{0.98}Pt_{0.02}O_{2-\delta}$	2	30			≥99.8, 300	4.5 (220)	0.04 (220)		[20]
$Ce_{0.98}Pt_{0.02}O_{2-\delta}$	2	30	50		95, 400	6.62 (280)	0.06 (280)	15	[20]
$Ce_{0.78}Sn_{0.2}Pt_{0.02}O_{2-\delta}$	3.8	25	36		>99, 300	11.1 (300)	0.09 (300)	6.7	[21]
$Ce_{0.95}Ru_{0.05}O_{2-\delta}$	5	30			≥99.8, 275	20.5 (275)	0.08 (275)	12.1	[44]
$Ce_{0.95}Ru_{0.05}O_{2-\delta}$	5	30	10	10	≥99.8, 305	14.5 (275)	0.06 (275)	12.6	[44]
$Ce_{0.95}Ru_{0.05}O_{2-\delta}$	5	30	40		≥99.8, 335	9.85 (275)	0.04 (275)	13.5	[44]
$Ce_{0.67}Fe_{0.33}O_{2-\delta}$	2	30			≥99.8, 275	2.8 (450)		33.8	Present work
$Ce_{0.65}Fe_{0.33}Pt_{0.02}O_{2-\delta}$	2	30			≥99.8, 275	4.05 (275)	0.031 (275)	12.1	Present work

compound was cooled to room temperature) for 12 h and restarted without any pretreatment of the catalyst for the next cycle. The WGS Reaction activity of the catalyst was completely repeatable and the complete conversion (~99%) of CO to CO_2 was observed with 100% H_2 selectivity achieved in each cycle. There was no measurable decrease in CO conversion or H_2 generation with the number of reaction cycles.

The spent catalyst ($Ce_{0.65}Fe_{0.33}Pt_{0.02}O_{2-\delta}$) after 10 cycles of WGS reactions was examined by XRD and XPS and the structure of the spent catalyst was refined by the Rietveld method [30]. The Rietveld refined powder XRD pattern of the spent $Ce_{0.65}Fe_{0.33}Pt_{0.02}O_{2-\delta}$ catalyst after 10 cycles of WGS reactions is shown in Fig. 1(c). All the peaks were indexed to fluorite structures and peaks corresponding to Fe_2O_3, FeO, PtO_2, PtO, or Pt metal impurities were not observed in the powder XRD pattern. A lattice parameter of the spent $Ce_{0.65}Fe_{0.33}Pt_{0.02}O_{2-\delta}$ catalyst after 10 cycles of WGS reactions was found to be 5.399 Å which is slightly higher compared to the lattice parameter (5.341 Å) of an as-prepared $Ce_{0.65}Fe_{0.33}Pt_{0.02}O_{2-\delta}$ catalyst subjected to a WGS reaction. Structural parameters of the spent $Ce_{0.65}Fe_{0.33}Pt_{0.02}O_{2-\delta}$ catalyst after 10 cycles of WGS reaction are given in Table 1. The rate and activation energy are comparable to other noble metal ionic catalysts. Pt free $Ce_{0.67}Fe_{0.33}O_{2-\delta}$ works at a high temperature with over 99% conversion and a high rate. The activation energy is about 3 times more than the corresponding Pt substituted catalyst.

The oxidation state of the metal ion with the spent $Ce_{0.65}Fe_{0.33}Pt_{0.02}O_{2-\delta}$ catalyst is determined by XPS. The core level Fe(2p) spectra of the spent $Ce_{0.65}Fe_{0.33}Pt_{0.02}O_{2-\delta}$ catalyst is shown in Fig. 3(c). Fe is mostly present in the 3+ oxidation state in the spent catalyst. However, the broader Fe($2p_{3/2}$) peak in the case of the spent catalyst (Fig. 3(c)) compared to the as-prepared catalyst (Fig. 3(b)) suggests that a small percentage of Fe^{2+} is present in the spent catalyst. The core level Ce(3d) spectra of the spent $Ce_{0.65}Fe_{0.33}Pt_{0.02}O_{2-\delta}$ catalyst is shown in Fig. 4(c). Ce was also found in a mixed valent (4+/3+) state in the spent catalyst. Similarly, more of Pt^{2+} states are found after the catalytic reactions as can be seen from Fig. 5(b). CO seems to keep the catalyst under mild reducing conditions during the WGS reaction. Thus the XPS study shows a slight reduction of the catalyst. The increase in the lattice parameter of the spent $Ce_{0.65}Fe_{0.33}Pt_{0.02}O_{2-\delta}$ catalyst compared to the as-prepared catalyst also confirms that the catalyst is slightly reduced after 10 cycles of WGS reactions. However, the XRD study still shows that the compound retained its crystal structure. Thus, the catalyst remained intact even after 10 cycles of WGS reactions and no decrease in the WGS activity of the catalyst was observed.

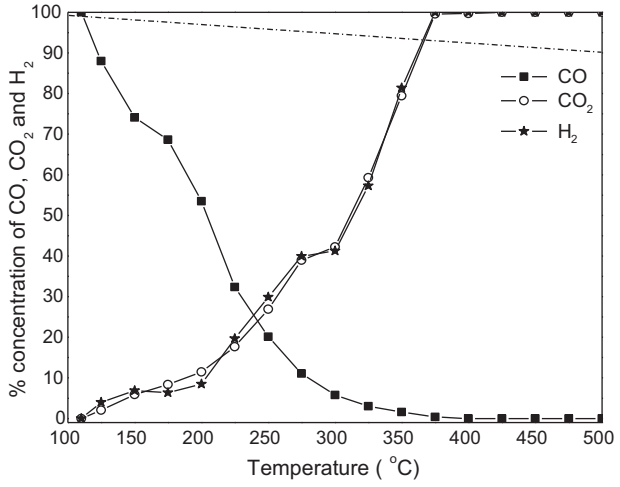

Fig. 14. %CO, CO_2 and H_2 concentrations in the WGS reaction with the feed gas composition (2 cm^3/min CO, 10 cm^3/min CO_2, 10 cm^3/min H_2, 30 cm^3/min H_2O balance with N_2 keeping total flow 130 cm^3/min with the $Ce_{0.65}Fe_{0.33}Pt_{0.02}O_{2-\delta}$ catalyst. Equilibrium CO_2 formation or CO conversion is given by dash-dot line.

4. Conclusions

In summary, a new low temperature sonochemical method is described here to prepare both Pt^{4+} and Fe^{3+} ion substituted ceria ($Ce_{0.65}Fe_{0.33}Pt_{0.02}O_{2-\delta}$) catalysts for low temperature CO oxidation and WGS reactions. Fe substituted ceria ($Ce_{0.67}Fe_{0.33}O_{2-\delta}$), itself acts as a good catalyst for CO oxidation and WGS reactions at moderate temperatures. Due to the synergistic interaction of the Pt ion with Ce and Fe ions in $Ce_{0.65}Fe_{0.33}Pt_{0.02}O_{2-\delta}$, the catalyst shows much higher activity for CO oxidation and WGS reactions compared to $Ce_{0.67}Fe_{0.33}O_{2-\delta}$. A strong synergistic interaction in the $Ce_{0.65}Fe_{0.33}Pt_{0.02}O_{2-\delta}$ catalyst was also observed by H_2/TPR or hydrogen uptake studies. Higher lattice oxygen removal at a lower temperature by H_2 or CO was observed with $Ce_{0.65}Fe_{0.33}Pt_{0.02}O_{2-\delta}$ (reduction peak at ~125 °C) when compared to $Ce_{0.67}Fe_{0.33}O_{2-\delta}$ (reduction peak at ~420 °C). Due to the presence of ionic Pt in $Ce_{0.65}Fe_{0.33}Pt_{0.02}O_{2-\delta}$, a reverse WGS reaction does not occur over the catalyst and a nearly complete conversion of CO to CO_2 with 100% H_2 selectivity is observed in WGS reactions even up to 550 °C.

References

[1] T. Bunluesin, R.J. Gorte, G.W. Graham, Appl. Catal. B: Environ. 15 (1998) 107.
[2] R.J. Gorte, S. Zhao, Catal. Today 104 (2005) 18.
[3] C.D. Zeinalipour-Yazdi, A.M. Efstathiou, J. Phys. Chem. C 112 (2008) 19030.
[4] S.-C. Huang, C.-H. Lin, J.H. Wang, J. Phys. Chem. C 114 (2010) 9826.
[5] N.L. Wieder, M. Cargnello, K. Bakhmutsky, T. Montini, P. Fornasiero, R.J. Gorte, J. Phys. Chem. C 115 (2011) 915.
[6] Q. Fu, H. Saltsburg, M. Flytzani-Stephanopoulos, Science 301 (2003) 935.
[7] Q. Fu, S. Kudriavtseva, H. Saltsburg, M. Flytzani-Stephanopoulos, Chem. Eng. J. 93 (2003) 41.
[8] W. Deng, J. De Jesus, H. Saltsburg, M. Flytzani-Stephanopoulos, Appl. Catal. A 291 (2005) 126.
[9] F.C. Meunier, D. Reid, S. Shekhtman, C. Hardcare, R. Burch, W. Deng, M. Flytzani-Stephanapoulos, Appl. Catal. B 247 (2007) 277.
[10] W. Deng, M. Flytzani-Stephanopoulos, Angew. Chem. Int. Ed. 45 (2006) 2285.
[11] D. Pierre, W. Deng, M. Flytzani-Stephanopoulos, Top. Catal. 46 (2007) 363.
[12] W. Deing, A.I. Frenkel, R. Si, M. Flytzani-Stephanopoulos, J. Phys. Chem. C 112 (2008) 12834.
[13] R. Si, M. Flytzani-Stephanopoulos, Angew. Chem. Int. Ed. 47 (2008) 2884.
[14] X. She, M. Flytzani-Stephanopoulos, C. Wang, Y. Wang, C.H.F. Peden, Appl. Catal. B 88 (2009) 98.
[15] N. Yi, R. Si, H. Saltsburg, M. Flytzani-Stephanopoulos, Appl. Catal. B 95 (2010) 87.
[16] Z. Zhou, M. Flytzani-Stephanopoulos, H. Saltsburg, J. Catal. 280 (2011) 255.
[17] M.B. Boucher, N. Yi, F. Gittleson, B. Zugic, H. Saltsburg, M. Flytzani-Stephanopoulos, J. Phys. Chem. C 115 (2011) 1261.
[18] I. Valsamakis, M. Flytzani-Stephanopoulos, Appl. Catal. B 106 (2011) 255.
[19] M.S. Hegde, G. Madras, K.C. Patil, Acc. Chem. Res. 42 (2009) 704.
[20] S. Sharma, P.A. Deshpande, M.S. Hegde, M. Giridhar, Ind. Eng. Chem. Res. 48 (2009) 6535.
[21] A. Gupta, M.S. Hegde, Appl. Catal. B: Environ. 99 (2010) 279.
[22] J.E. Huheey, Inorganic Chemistry, Principles of Structure and Reactivity, 3rd ed., Harper and Row, New York, 1983, p. 129.
[23] T. Baidya, A. Gayen, M.S. Hegde, N. Ravishankar, L. Dupont, J. Phys. Chem. B 110 (2006) 5262.
[24] T. Baidya, A. Marimuthu, M.S. Hegde, N. Ravishankar, G. Madras, J. Phys. Chem. C 111 (2007) 830.
[25] T.B. Nguyen, J.P. Deloume, V. Perrichon, Appl. Catal. A 249 (2003) 273.
[26] T. Baidya, A. Gupta, P.A. Deshpandey, G. Madras, M.S. Hegde, J. Phys. Chem. C 113 (2009) 4059.
[27] H. Bao, X. Chen, J. Fang, Z. Jiang, W. Huang, Catal. Lett. 125 (2008) 160.
[28] A. Penkova, K. Chakarova, O.H. Laguna, K. Hadjiivanov, F. Romero Saria, M.A. Centeno, J.A. Odriozola, Catal. Commun. 10 (2009) 1196.
[29] T. Tabakova, M. Manzoli, D. Paneva, F. Boccuzzi, V. Idakiev, I. Mitov, Appl. Catal. B 101 (2011) 266.
[30] P. Singh, M.S. Hegde, Dalton Trans. 39 (2010) 10798.
[31] T. Roisnel, J. Rodríguez-Carvajal, Mater. Sci. Forum 118 (2001) 378.
[32] B.D. Cullity, Elements of X-ray Diffraction, 2nd ed., Addison-Wesley, Reading, MA, 1978, p. 281.
[33] G. Caglioti, A. Paoletti, F.P. Ricci, Nucl. Instrum. Methods 3 (1958) 223.
[34] C.N.R. Rao, D.D. Sarma, S. Vasudevan, M.S. Hegde, Proc. R. Soc. Lond. A 367 (1979) 239.
[35] A. Kotani, H. Ogasawara, J. Electron Spectrosc. Relat. Phenom. 60 (1992) 257.
[36] J.S. Hammond, N. Winograd, J. Electroanal. Chem. 78 (1977) 55.
[37] C.J. Powell, P.E. Larson, Appl. Surface Sci. 1 (1978) 186.
[38] J.H. Scofield, J. Electron Spectrosc. Relat. Phenom. 8 (1976) 129.
[39] D.R. Penn, J. Electron Spectrosc. Relat. Phenom. 9 (1976) 29.
[40] G. Dutta, U.V. Waghmare, T. Baidya, M.S. Hegde, Chem. Mater. 19 (2007) 6430.
[41] P. Singh, M.S. Hegde, Cryst. Growth Des. 10 (2010) 2995.
[42] J.M. Moe, Chem. Eng. Pro. 58 (1962) 33.
[43] X. Liu, W. Ruettinger, X. Xu, R. Farrauto, Appl. Catal. B: Environ. 56 (2005) 69.
[44] P. Singh, N. Mahadevaiah, S.K. Parida, M.S. Hegde, J. Chem. Sci., in press.